J. Fluid Mech. (1982), *vol.* 122, *pp.* 155–167
Printed in Great Britain

Cloud patterns around a bubble growing in a gas-fluidized bed

By R. COLLINS

Department of Mechanical Engineering,
University College London,
Torrington Place, London WC1E 7JE

(Received 20 October 1981)

The gas-flow pattern that occurs when a bubble grows during its passage through a fluidized bed is investigated by applying Davidson's (1961) model in an unsteady manner. It is found that the form of the cloud perceived by an observer of this unsteady motion is significantly different from that predicted by the steady theory. Growth is shown to lead to a reduction in the penetration of the cloud ahead of the bubble and a reduction in the area of overlap between cloud and particles. The cloud boundary also intercepts the bubble boundary, and the gas entering the bubble to sustain its growth does so through its base. There is good agreement with experimental observation of clouds.

1. Introduction

Davidson's (1961) model of a bubble in a fluidized bed was the first to predict the gas cloud that forms around the bubble when its velocity exceeds the interstitial gas velocity into the bed. Several current models of chemical reaction in fluidized beds now consider reactions within the cloud and emulsion phases separately, so that it is clearly important to know how much gas is invested in the cloud at any instant. Figure 1(*a*) shows Rowe, Partridge & Lyall's (1964) comparison of cloud shapes predicted theoretically for circular two-dimensional bubbles moving steadily and a typical shape observed experimentally using NO_2 as a tracer gas. As far as the distance to which the cloud penetrates the particle flow ahead of the bubble is concerned, the data of Rowe *et al.*, although scattered, favoured Murray's (1965*a*, *b*) theory, which took into account an equation of motion for the particles, but both theories appear to be seriously deficient in their descriptions of the cloud shape behind the bubble. The most obvious difference shown in figure 1(*a*) is that real clouds appear to intersect the bubble boundary, while the theoretical cloud boundaries always surround it. It might be thought that the reason for this discrepancy could be found in the fact that real bubbles are not circular, but studies of non-circular bubbles using both theories have not reproduced this aspect of real cloud behaviour, although they do indicate reductions in cloud volume from the values obtained for circular bubbles (Collins 1965; Murray 1965*a*, *b*; Stewart 1968; Clift *et al.* 1972). Rowe *et al.* observed also that gas can be shed from the sides of the cloud in lobes of characteristic form (shown here in figure 2), and they noted that this feature was also not described by the theories with which their comparisons were made. Their experiments were set up and performed with great care and skill, and they sought to reproduce the condition of steady motion

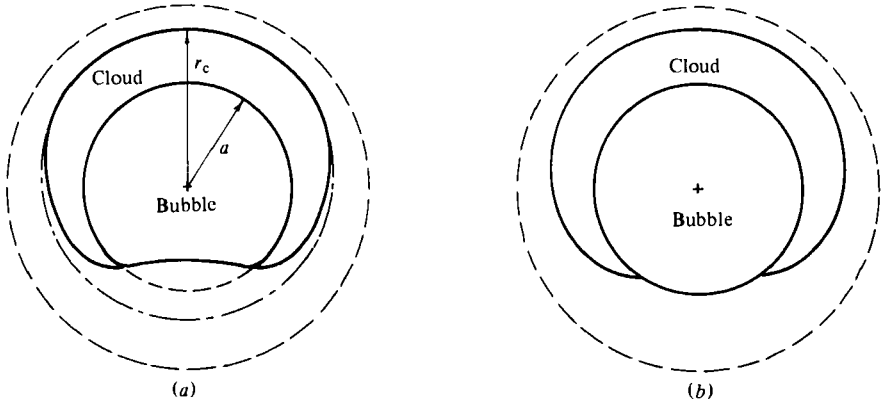

FIGURE 1. (*a*) Rowe, Partridge & Lyall's (1964) comparison of experimental and steady theoretical cloud shapes for $\alpha = 2$. – – –, Davidson (1961); – · – · –, Murray (1965*a*, *b*); ——, experimental cloud. (*b*) Cloud shapes for $\alpha = 2$. – – –, Davidson's (1961) steady solution; ——, growing bubble, this work with $\gamma = 0{\cdot}26$.

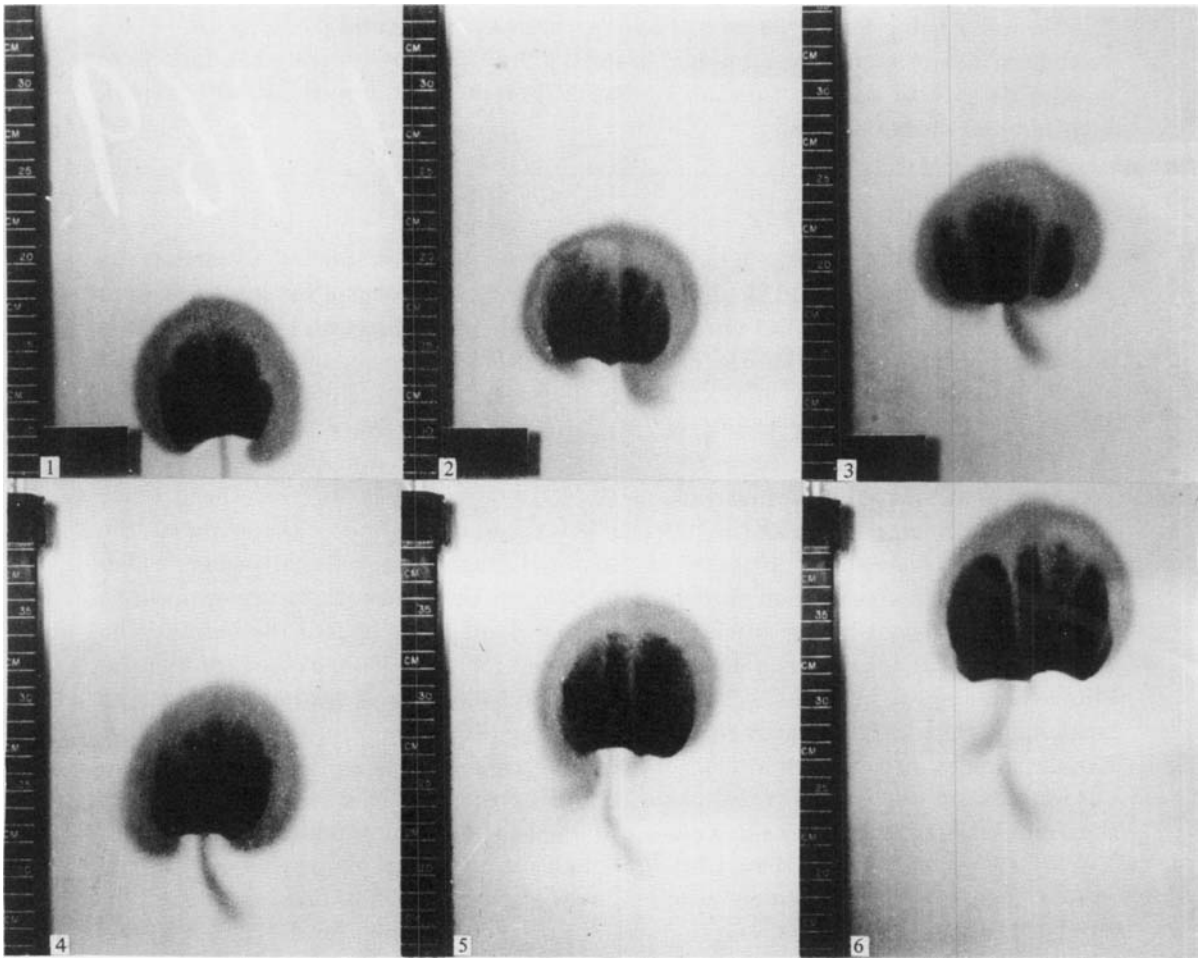

FIGURE 2. Experimental cloudforms in a two-dimensional bed from the experiments of Rowe *et al.* (1964); $\alpha \cong 2{\cdot}5$.

assumed in the theories, but it will be clear from figure 2 that the natural experimental motion is essentially unsteady. Unsteadiness can arise in a number of forms, not all of which are present in figure 2: for example there can be changes in bubble shape, velocity, orientation and path as well as the evident change in size. Recently Collins (1980) has shown that incorporation of some of these unsteady features, namely yaw, surge and sway, into Davidson's model can lead to shedding phenomena like those shown in figure 2. In this paper it is shown that if bubble growth is considered in the context of Davidson's model then significant changes in the gas flow pattern occur, and these changes are consistent with the real cloud behaviour shown in figure 1 (*a*). Specifically it is found that

(i) the cloud penetration ahead of the bubble is reduced by bubble growth;

(ii) the cloud intercepts the bubble boundary;

(iii) the gas entering the bubble to sustain its growth does so through its base.

With a rate of growth sufficient to reduce the cloud penetration to values which are consistent with Murray's theory, and hence with the experiments of Rowe *et al.*, the cloud has the typical shape shown in figure 1 (*b*). The area of overlap between cloud and particles is found to be substantially reduced by bubble growth.

2. Theory

The gas and particle phases are treated in Davidson's theory as incompressible continuous media which interact according to Darcy's law so that

$$\operatorname{div}\mathbf{u} = 0, \quad \operatorname{div}\mathbf{v} = 0, \tag{1), (2}$$

$$\mathbf{u} - \mathbf{v} = -k \operatorname{grad} p, \tag{3}$$

where $\mathbf{u}$ and $\mathbf{v}$ are the gas and particle velocity vectors, p is the gas pressure, and k is considered to be constant. Davidson applied these equations originally to the problem of steady motion of a circular or spherical bubble, but it was later observed (Davidson & Harrison 1966) that the equations apply also when the motion is unsteady, provided that the voidage in the particle phase is constant. Davidson & Harrison used this result to study the division of total gas flow between bubble and interstitial phases in a freely bubbling bed, and Collins (1980) has recently used it to describe cloud patterns around isolated bubbles that move with yaw, surge and sway. From (1)–(3) we have

$$\operatorname{div} \operatorname{grad} p = 0, \tag{4}$$

which shows that, for given boundary conditions on p, the gas pressure distribution is unaffected by the particle motion, and hence from (3)

$$\mathbf{u} = \mathbf{u}_0 + \mathbf{v}, \tag{5}$$

where $\mathbf{u}_0$ is the gas velocity that would exist if the particles were stationary. This result holds for both steady and unsteady motions with constant voidage, and it enables us to determine the gas velocity field at any instant in an unsteady motion by superimposing two constituents: (i) the particle velocity field, and (ii) the gas velocity field that would exist at that instant if the particles were fixed.

Irrotational motions are taken to describe both constituent flows so that

$$\phi_G = \phi_{G0} + \phi_P, \tag{6}$$

where ϕ is the velocity potential, with suffixes G and P denoting gas and particles respectively. The potential for the constituent gas motion is clearly $\phi_{G0} = -kp$ from (3). This paper will concentrate on flow patterns for two-dimensional motions, since they are capable of experimental observation.

Consider a circular bubble rising and growing without change of shape. Axes are fixed on the bubble, with the positive x-direction vertically upwards, the bubble velocity is denoted by U_B, its radius a increases at a rate $\dot{a}$ and the interstitial gas velocity into the bed and remote from the bubble is U_G. The two potential problems which arise for solution and superposition are then as follows.

For the particles (problem A)

$$\nabla^2\phi_P = 0, \tag{7}$$

with boundary conditions

$$\left.\begin{aligned} &\partial\phi_P/\partial x \to -U_B \quad \text{as} \quad r \to \infty, \\ &\partial\phi_P/\partial r = \dot{a} \quad \text{on} \quad r = a. \end{aligned}\right\} \tag{8}$$

For the constituent gas motion (problem B)

$$\nabla^2\phi_{G0} = 0, \tag{9}$$

with boundary conditions

$$\left.\begin{aligned} &\partial\phi_{G0}/\partial x \to U_G \quad \text{as} \quad r \to \infty, \\ &\phi_{G0} = \text{constant} \quad \text{on} \quad r = a. \end{aligned}\right\} \tag{10}$$

The acyclic solution of problem A is

$$\phi_P = -U_B(r + a^2/r)\cos\theta + a\dot{a}\log r, \tag{11}$$

which consists of a streaming motion past the bubble with an additional source term representing the radial velocity field produced by bubble growth. In the steady theory (Davidson 1961) the solution of problem B was taken to be

$$\phi_{G0} = U_G(r - a^2/r)\cos\theta, \tag{12}$$

which represents percolation into a stationary void in an infinite porous mass. For the purposes of the present theory, however, it is necessary to note that the solution of problem B is not unique, because a term representing a sink, of strength m say, may be added to (12) without affecting the boundary conditions so that

$$\phi_{G0} = U_G(r - a^2/r)\cos\theta - (m/2\pi)\log r. \tag{13}$$

This sink term must be included here in order to deliver to the bubble the gas flow that will result in its growth,† and it follows that the sink strength is such that $m = 2\pi a\dot{a}/\epsilon$, where ϵ is the voidage in the particle phase. Inside the bubble it is assumed that $\epsilon = 1$. The potential for the gas flow associated with a growing bubble obtained from (6), (11) and (13) is therefore

$$\phi_G = -U_G\{(\alpha - 1)r + (\alpha + 1)a^2/r\}\cos\theta - (a\dot{a}(1-\epsilon)/\epsilon)\log r, \tag{14}$$

where $\alpha = U_B/U_G$. When expressed in terms of a complex potential $w_G = \phi_G + i\psi_G$ we obtain

$$w_G = -U_G\{(\alpha - 1)z + (\alpha + 1)a^2/z + a\gamma\log z\}, \tag{15}$$

† Without the sink in (13), superposition of (11) and (12) would imply the presence of a net source of gas within the bubble in the resulting gas flow.

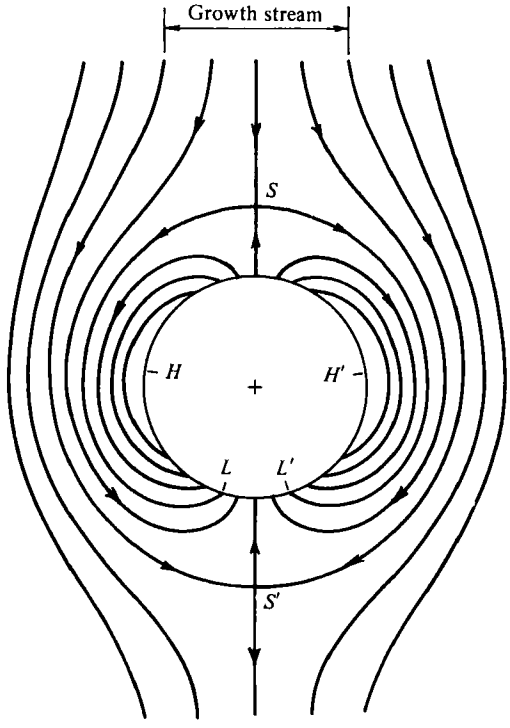

FIGURE 3. Instantaneous streamline pattern associated with a growing bubble; $\alpha = 2, \gamma = 0{\cdot}2$.

where $\gamma = (1-\epsilon)\,\dot{a}/\epsilon U_G$ is a parameter describing the growth rate. Davidson's steady theory has $\gamma = 0$, and the steady streamline $\psi_G = 0$ from (15) then defines a cloud which forms when $\alpha > 1$ and is concentric with the bubble with radius r_c given by

$$\frac{r_c}{a} = \left(\frac{\alpha+1}{\alpha-1}\right)^{\frac{1}{2}}. \tag{16}$$

Figure 1 (*a*) shows this cloud for $\alpha = 2$; the area of the region of overlap of cloud and particles in this case is found from (16) to be

$$S_0 = 2\pi a^2/(\alpha-1). \tag{17}$$

When $\gamma \neq 0$, (15) defines a pattern of instantaneous streamlines whose character is shown in figure 3 for the values $\alpha = 2, \gamma = 0{\cdot}2$. The gas responsible for bubble growth is evidently drawn from a channel ahead of the bubble whose asymptotic width is found to be $2\pi a\gamma/(\alpha-1)$ from (15) but, because gas flows out of the bubble roof over the arc HH', this growth stream is deflected around the bubble and enters through its base over the arc LL'. The gas efflux from the bubble roof produces an instantaneous stagnation point (relative to axes fixed on the bubble centre) at S, while the collection of the growth stream at the bubble rear leads to an instantaneous stagnation point at S'. From the derivative of (15), the locations of these points on the x-axis, which will be denoted by r_s, are at the roots of the quadratic

$$r_s^2(\alpha-1) + r_s\,a\gamma - a^2(\alpha+1) = 0, \tag{18}$$

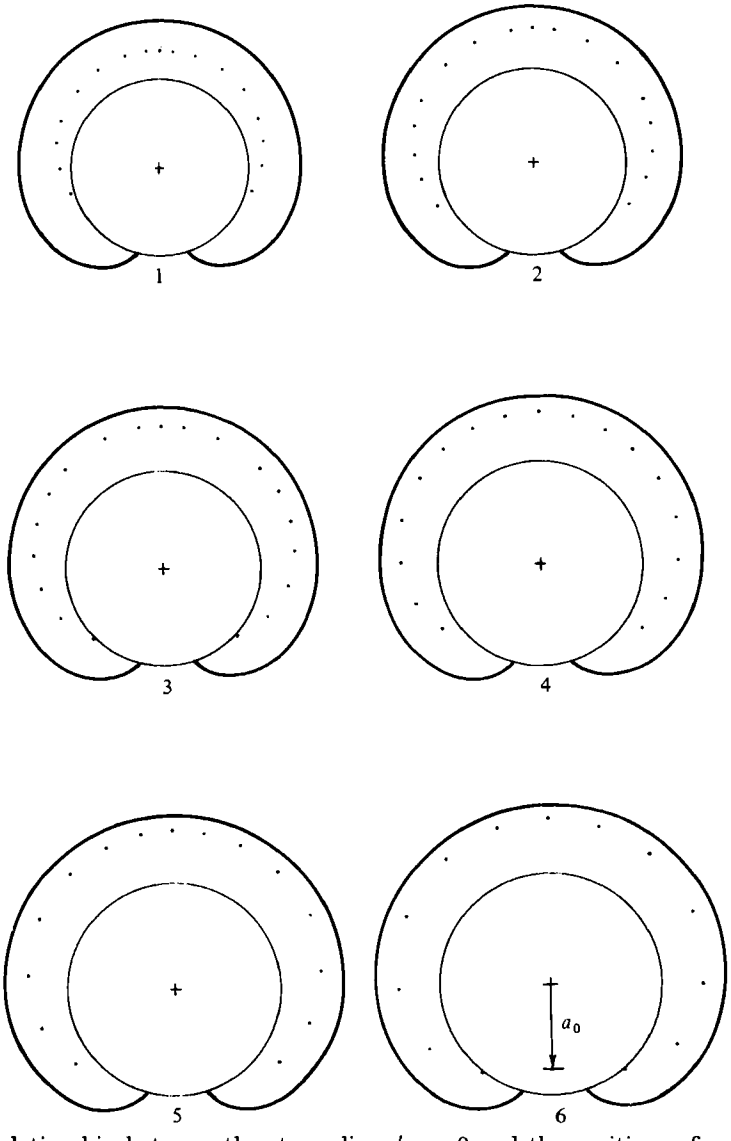

FIGURE 4. Relationship between the streamline $\psi_G = 0$ and the positions of marked gas elements located initially on the bubble boundary; $\alpha = 2$, $\gamma = 0{\cdot}2$, $\epsilon = 0{\cdot}4$. ——, streamline $\psi_G = 0$; · · · ·, current positions of marked elements. The initial bubble radius is a_0, the distance travelled by the bubble centre between images is $0{\cdot}75a_0$.

that is where

$$\frac{r_s}{a} = \pm\left\{\frac{\alpha+1}{\alpha-1} + \left[\frac{1}{2}\frac{\gamma}{\alpha-1}\right]^2\right\}^{\frac{1}{2}} - \frac{1}{2}\frac{\gamma}{\alpha-1}. \tag{19}$$

The linearized form of (19), namely

$$\frac{r_s}{a} = \pm\left\{\frac{\alpha+1}{\alpha-1}\right\}^{\frac{1}{2}} - \frac{1}{2}\frac{\gamma}{\alpha-1}, \tag{20}$$

shows that, to first order, the stagnation points are displaced downwards through a

distance $\frac{1}{2}a\gamma/(\alpha-1)$ from their positions for the steady state at this value of α (cf. (16)). The curved branch of the instantaneous streamline $\psi_G = 0$ passes through S and has the equation

$$r^2(\alpha-1)+ra\gamma\theta/\sin\theta-a^2(\alpha+1) = 0. \tag{21}$$

It intersects the bubble boundary at L and L', so defining the arc length over which the growth stream enters the bubble. This arc subtends an angle 2χ at the bubble centre, where

$$\sin\chi = \tfrac{1}{2}\gamma(\pi-\chi), \tag{22}$$

which gives

$$\chi = \tfrac{1}{2}\gamma\pi, \tag{23}$$

to first order in γ. The arc length is independent of α and is constant for a constant growth-rate parameter γ. The instantaneous streamline $\psi_G = 0$ is changing continually, and gas which has once entered the bubble is trapped behind this line; in this unsteady motion, however, it does not represent the boundary of a cloud as it does in the steady case, although, as will be shortly apparent, there can be a close similarity. The boundary of the cloud perceived by an observer of the motion separates what may be described as 'old' gas which has been captured by the bubble (and which would be coloured experimentally by mixing with NO_2) and new gas which is clear. To find the location of this boundary and to show its relationship with the streamline $\psi_G = 0$ it is necessary to do numerical work on (15) in order to follow the paths of marked elements of gas throughout the motion. For simplicity we take α and γ to be constants so that the form of the instantaneous streamline pattern does not change; it is only altered in scale as the bubble expands with constant $\dot{a}$. For $\alpha = 2$, $\gamma = 0{\cdot}2$ and $\epsilon = 0{\cdot}4$, figure 4 shows the positions at six subsequent times of marker elements of gas which were located on the bubble boundary $r = a_0$ at the initial instant. The constituents of this figure were obtained from a modified form of the computer-graphics program developed to produce animated sequences of the cloud patterns that arise owing to yawing, surging and swaying motions of the bubble (Collins 1980). It may be seen that the marker elements (representing gas dyed with NO_2) rapidly adopt locations close to the streamline $\psi_G = 0$ but always contained by it. The marker starting from the bubble apex does not reach the instantaneous stagnation point at S, the location of which is itself advancing relative to the bubble centre at a velocity greater than $\dot{a}$, but it appears to settle to the position on the x-axis where the local instantaneous gas velocity relative to the bubble centre is equal to the velocity of the bubble apex relative to the same datum, that is $\dot{a}$. On this basis the distance to the cloud front from the origin obtained from the derivative of (15) and denoted by r_c is given by the positive root of the quadratic

$$r_c^2(\alpha-1+\gamma\epsilon/(1-\epsilon))+r_c a\gamma-a^2(\alpha+1) = 0, \tag{24}$$

namely

$$\frac{r_c}{a} = \left\{\frac{\alpha+1}{\alpha-1+\gamma\epsilon/(1-\epsilon)}+\left[\frac{1}{2}\frac{\gamma}{\alpha-1+\gamma\epsilon/(1-\epsilon)}\right]^2\right\}^{\frac{1}{2}}-\frac{1}{2}\frac{\gamma}{\alpha-1+\gamma\epsilon/(1-\epsilon)}. \tag{25}$$

On retaining only the linear terms in γ, (25) gives

$$\frac{r_c}{a} = \left(\frac{\alpha+1}{\alpha-1}\right)^{\frac{1}{2}}\left\{1-\frac{1}{2}\frac{\gamma}{\alpha-1}\frac{\epsilon}{1-\epsilon}\right\}-\frac{1}{2}\frac{\gamma}{\alpha-1}, \tag{26}$$

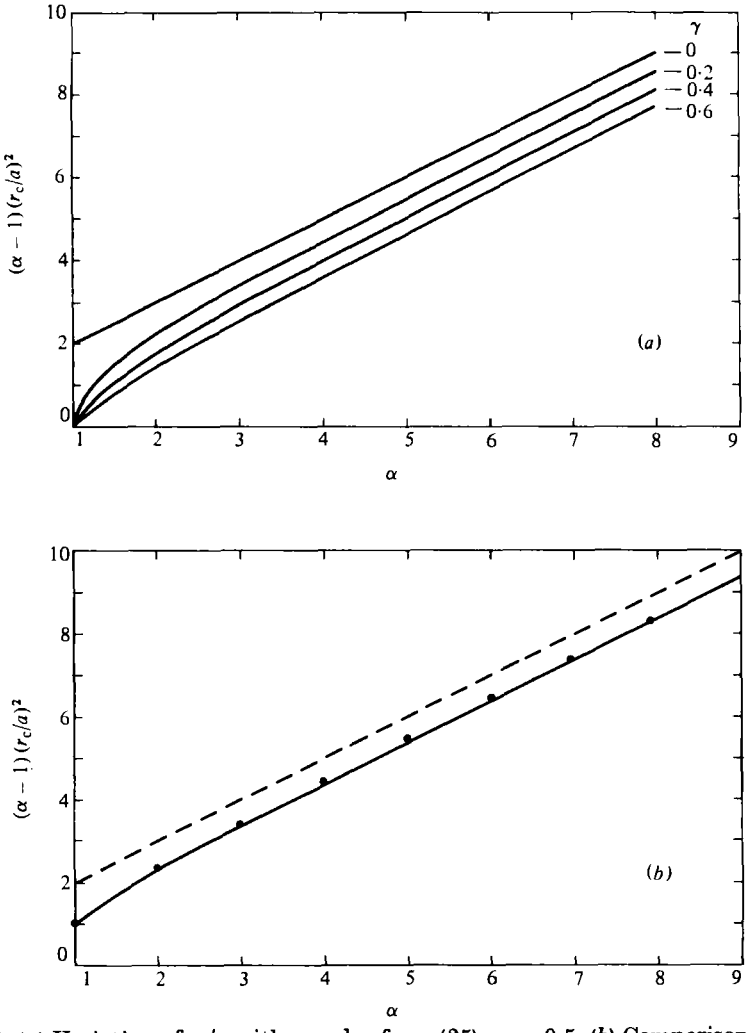

FIGURE 5. (*a*) Variation of r_c/a with α and γ from (25); $\epsilon = 0{\cdot}5$. (*b*) Comparison of cloud dimensions. – – –, Davidson's (1961) steady solution; ●, Murray (1965*a*, *b*); ——, this work with $\gamma = 0{\cdot}3\{(\alpha-1)(1-\epsilon)/\epsilon(\alpha+1)\}^{\frac{1}{2}}$; $\epsilon = 0{\cdot}5$. (The effect of changes in ϵ in the range $0{\cdot}4 < \epsilon < 0{\cdot}8$ is very weak and is not shown for clarity.)

which indicates that, for given α, bubble growth acts to reduce the extent of the penetration of the cloud into the particle flow. For comparative purposes it is convenient to take $\epsilon = 0{\cdot}5$, so that the term $\epsilon/(1-\epsilon) = 1$, and for this value figure 5(*a*) shows the cloud dimension r_c obtained from (25) for several values of γ. This figure confirms that, in an instantaneous experimental comparison effected at a given value of α, the presence of growth would be expected to produce cloud sizes smaller than those given by Davidson's steady theory; the cloud boundary, moreover, intercepts the bubble boundary. These findings are consistent with the observations of Rowe *et al.* Their measurements of r_c were compared with two steady theories, and they were found to favour Murray's steady equation

$$r_c^3(\alpha-1) - \alpha r_c a^2 - \tfrac{1}{2}a^3 = 0, \tag{27}$$

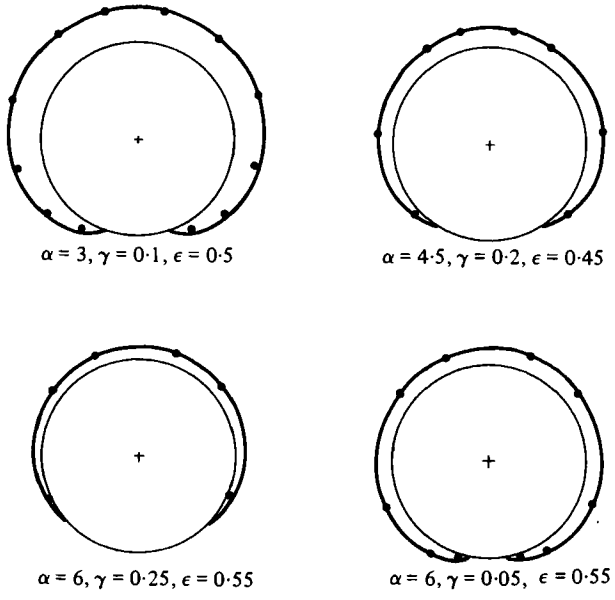

FIGURE 6. Comparison of approximate equation for cloud shape and the cloud form obtained from computer-graphics sequences. ——, equation (29); ●, positions of marked elements. (Marker sizes are exaggerated for the purposes of this figure.)

with the cloud shape shown in figure 1(*a*). For the present purpose we may take this equation to represent a mean line through the experimental data, and figure 5(*b*) shows that it is virtually coincident with the line obtained from the present unsteady theory when the growth-rate parameter γ adopts values given by

$$\gamma = 0{\cdot}3\left\{\frac{\alpha-1}{\alpha+1}\right\}^{\frac{1}{2}}\left\{\frac{1-\epsilon}{\epsilon}\right\}^{\frac{1}{2}}. \tag{28}$$

In the data obtained from experiments of this type scatter is inevitable, and it would not be possible in fact to distinguish experimentally between the line given by (28) and that given by $\gamma \simeq 0{\cdot}2$ shown in figure 5(*a*).

There is no exact expression available to describe the rest of the cloud boundary defined by the positions of the other markers, but fortunately the apparent shape does not differ radically from the shape of the streamline $\psi_G = 0$ and, as a result, a very good approximation may be obtained by scaling (21) in a particular manner. A comparison between the linearized equations (26) and (20) suggests that the cloud penetration on the axis behaves effectively as if γ in (20) has been replaced by $\gamma[1+(\epsilon/(1-\epsilon))((\alpha+1)/(\alpha-1))^{\frac{1}{2}}]$. If we make the same replacement in (21), then the approximate description of the cloud becomes

$$\left.\begin{aligned} r^2(\alpha-1)+ra\gamma^*\theta/\sin\theta-a^2(\alpha+1) &= 0,\\ \text{with}\qquad \gamma^* &= \gamma\left[1+\left\{\frac{\alpha+1}{\alpha-1}\right\}^{\frac{1}{2}}\frac{\epsilon}{1-\epsilon}\right]. \end{aligned}\right\} \tag{29}$$

The utility of this approximate description may be gauged from the comparisons made in figure 6, which show that (29) describes the positions of marker elements obtained from computer-generated sequences very well in a variety of combinations

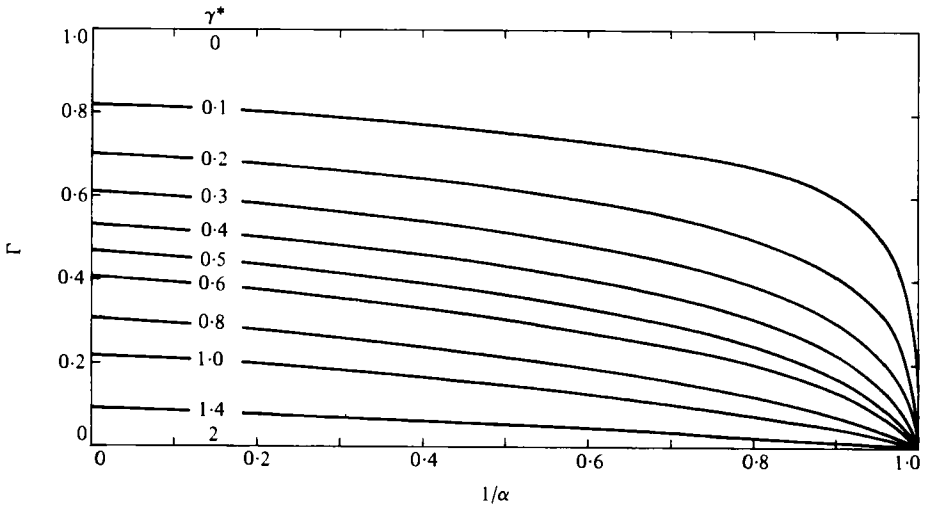

FIGURE 7. Variation of cloud overlap ratio Γ with $1/\alpha$ and γ^*.

of α, γ and ϵ. The approximation is less successful near $\alpha = 1$; its useful range is for $\alpha \gtrsim 1{\cdot}5$.

In the experiments of Rowe *et al.* a typical value of voidage was $\epsilon = 0{\cdot}4$. For $\alpha = 2$, (28) then gives $\gamma = 0{\cdot}26$, and the cloud shape for this combination obtained from (29) has been plotted in figure 1(*b*). Qualitative agreement with the typical experimental form in figure 1(*a*) is very good. Clearly, bubble growth leads to a significant reduction in the amount of gas present in the cloud overlap region, and we may estimate this from (29) by evaluating the area of the overlap, $S = \int_0^{\omega} (r^2 - a^2)\, d\theta$, where ω is the angular location of the intercept of cloud and bubble. When only linear terms in γ^* are retained, the area of the overlap is found to be

$$S = S_0 \left[1 - \tfrac{1}{2}\gamma^* - \frac{1}{2}\left\{\frac{\alpha+1}{\alpha-1}\right\}^{\frac{1}{2}} \frac{\gamma^*}{\pi} \int_0^{(1-\frac{1}{2}\gamma^*)\pi} \frac{\theta}{\sin\theta}\, d\theta \right], \tag{30}$$

where (17) and (20) have been used.

It may be shown that as $\gamma^* \to 0$

$$-\frac{\gamma^*}{\pi} \int_0^{(1-\frac{1}{2}\gamma^*)\pi} \frac{\theta}{\sin\theta}\, d\theta \sim \gamma^* \log \gamma^* - \gamma^* \sum_{n=1}^{\infty} (-1)^n \pi^{2n} / (2n+1)!\, 2n(2n+1)$$
$$\sim \gamma^* \log \gamma^* - 0{\cdot}238\gamma^*, \tag{31}$$

so that the asymptotic form of the cloud overlap ratio due to growth, denoted by $\Gamma = S/S_0$, is given by

$$\Gamma \sim 1 + \frac{1}{2}\left\{\frac{\alpha+1}{\alpha-1}\right\}^{\frac{1}{2}} \gamma^* \log \gamma^* - \tfrac{1}{2}\gamma^* \left[1 + 0{\cdot}238 \left\{\frac{\alpha+1}{\alpha-1}\right\}^{\frac{1}{2}} \right] \tag{32}$$

as $\gamma^* \to 0$. For general values of γ^*, the cloud overlap ratio has been evaluated without linearization by numerical integration, and the results are shown in figure 7. It is clear from this figure that the effect of growth in reducing Γ can be very large (for high values of α, $\Gamma \simeq 0{\cdot}4$ when $\gamma^* \simeq 0{\cdot}5$ for example), and changes of this magnitude brought about by the capture of gas from the growth stream ahead of the bubble

combined with the dilution of cloud gas by the same mechanism will have important consequences for gas contacting in the bed. Other features apparent from figure 7 are that Γ is relatively insensitive to α when $\alpha \gtrsim 2$, and that $\Gamma = 0$ for all values of α if $\gamma^* > 2$. The latter result implies that no cloud can form if the growth rate exceeds a certain value, because the growth stream then enters the bubble over the whole of its perimeter. The maximum value of γ involved may be obtained by setting $r_c/a = 1$ in (24), which gives $\gamma = 2(1-\epsilon)$. We observe that these maximum values of γ and γ^* are consistent with the relationship proposed in (29), provided that α is large.

3. Concluding remarks

The approach of the preceding work has been to use the experimental data of Rowe *et al.*, expressed through (28), to estimate the growth-rate parameter γ that would make Davidson's model consistent with experiments in respect of the cloud penetration distance r_c. In doing that, the effects of other features known to lead to some reduction in r_c, such as the presence of the wake fraction and of neighbouring walls, have not been taken into account, so that γ is slightly overestimated by this approach. The growth rates so found are generally modest and are consistent with those observable in figures such as figure 2. For example, (28) implies

$$\frac{\dot{a}}{U_B} = \frac{0{\cdot}3}{\alpha}\left\{\frac{\alpha-1}{\alpha+1}\frac{\epsilon}{1-\epsilon}\right\}^{\frac{1}{2}}, \tag{33}$$

which gives $\dot{a} = 0{\cdot}058U_B$ if $\alpha = 3$ and $\epsilon = 0{\cdot}4$, so that, in moving a distance of say $6a_0$, such a bubble would increase in radius by around 35 %. Under these conditions, the area of cloud overlap at any stage would be only about 40 % of that predicted by the steady theory.

For convenience this paper has considered the case when both α and γ are constants, but if the gas-flow patterns are to be followed with the computer this restriction can be easily removed. Variations in α, representing surge, have been studied previously (Collins 1980), and an example of the effect of a small surge on the cloud form is shown in figure 8(*a*). In all examples shown in this figure the marker elements were considered to be situated initially on the boundary of the cloud given by Davidson's steady solution, and the bubbles have moved a distance of $6a_0$ from this initial configuration. The computer-graphics output gives a series of illuminated points which represent the locations of the markers and of the bubble boundary, and the markers are made to appear to flow as the sequences are animated. To aid interpretation in the stills that form figure 8, the cloud markers have been joined by lines added manually. A periodic variation in γ leads to patterns generally similar to those found for surge as shown in figure 8(*a*), that is there is shedding of gas from the cloud in a lobe aligned along the line of motion. An interesting extreme example is shown in figure 8(*d*) for a high value of α coupled with a periodic variation in γ sufficient to produce peak-amplitude changes in bubble radius of only $\pm 0{\cdot}01a_0$. The effect is to shed gas from the cloud at a rate which makes it appear that gas is simply leaking out of the cloud along the line of motion. Rowe *et al.* record that this is a general feature of the patterns they observed at high values of α. These are, however, not the only two processes that can lead to gas shedding; figures 8(*b*, *c*) show shedding due to yaw, and to sway, and it will be clear that a superimposition of such perturbations with a

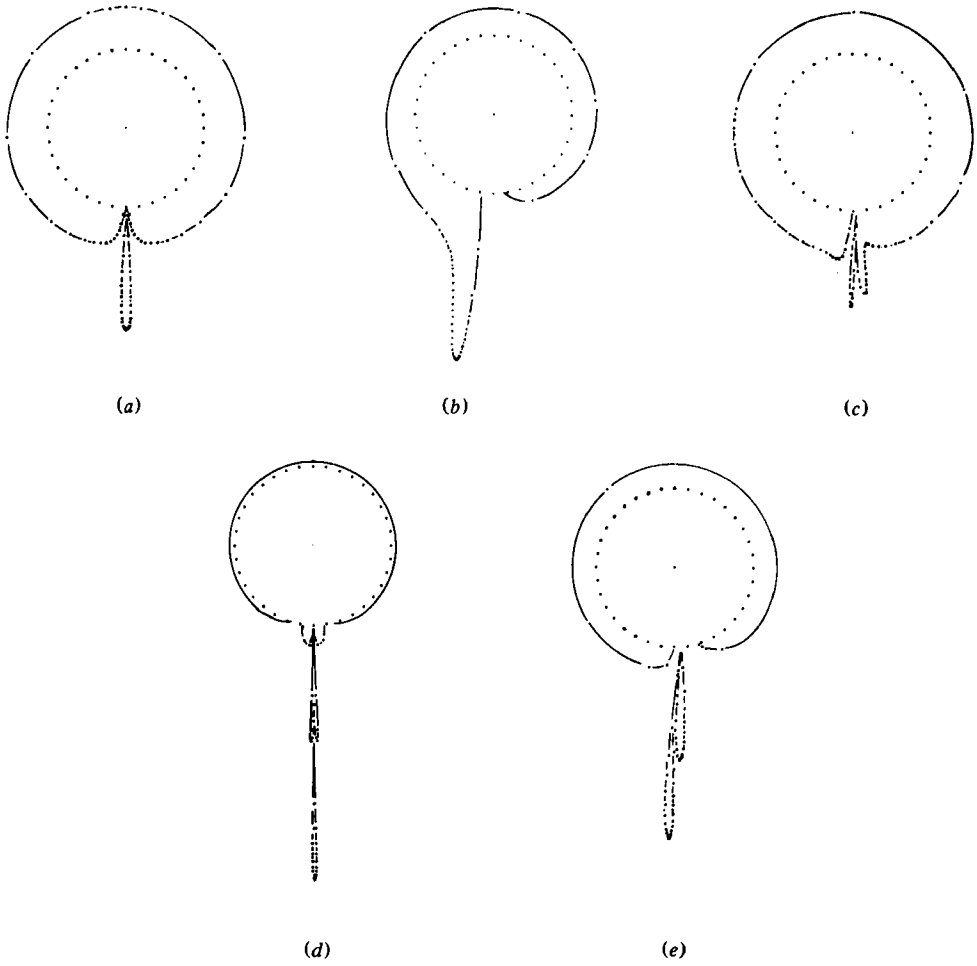

FIGURE 8. Examples of cloud patterns resulting from several unsteady influences. The bubble has moved a distance $6a_0$ from its initial position in each case. — · —, boundary of cloud and shed gas; · · ·, bubble boundary. (*a*) Surge; one half-cycle, maximum perturbation $+0{\cdot}1\alpha$, $\alpha = 2{\cdot}5$. (*b*) Yaw; bubble path at arctan 0·1 to the vertical, $\alpha = 3{\cdot}5$. (*c*) Sway; one cycle, maximum horizontal displacements $\pm 0{\cdot}25a_0$, $\alpha = 2{\cdot}5$. (*d*) Periodic growth; three cycles, maximum perturbations $\pm 0{\cdot}01a_0$, $\alpha = 20$. (*e*) Combined yaw, surge and sway; $\alpha = 4$.

multiplicity of possible combinations of amplitudes, phases and durations will be able to produce patterns of great complexity. An example stemming from a combination of yaw, surge and sway is shown in figure 8(*e*). It would seem that there is a great deal of information on gas exchange yet to be obtained from Davidson's theory applied in an unsteady manner. In addition to the influences already mentioned, it should be possible for example to consider the effects due to the growth of bubbles of non-circular form trailing a wake fraction, the effect of particle transfer to and from the wake fraction, and the gas exchange that occurs during bubble formation.

I am indebted to Mr E. Lyall and Mr B. A. Partridge of A.E.R.E., Harwell for providing the photographs shown in figure 2.

REFERENCES

CLIFT, R., GRACE, J. R., CHEUNG, L. & DO, T. H. 1972 *J. Fluid Mech.* **51**, 187.

COLLINS, R. 1965 *Chem. Engng Sci.* **20**, 747.

COLLINS, R. 1980 In *Proc. Int. Conf. on Fluidization, Henniker, N.H.* (ed. J. R. Grace & J. Matsen), pp. 24–32. Plenum.

DAVIDSON, J. F. 1961 *Trans. Inst. Chem. Engrs* **39**, 230.

DAVIDSON, J. F. & HARRISON, D. 1966 *Chem. Engng Sci.* **21**, 731.

MURRAY, J. D. 1965*a* *J. Fluid Mech.* **21**, 337.

MURRAY, J. D. 1965*b* *J. Fluid Mech.* **22**, 57.

ROWE, P. N., PARTRIDGE, B. A. & LYALL, E. 1964 *Chem. Engng Sci.* **19**, 973.

STEWART, P. S. B. 1968 *Trans. Inst. Chem. Engrs* **45**, 60.